Increased G_s Signaling in Osteoblasts Reduces Bone Marrow and Whole-Body Adiposity in Male Mice

Corey J. Cain, Joel T. Valencia, Samantha Ho, Kate Jordan, Aaron Mattingly, Blanca M. Morales, and Edward C. Hsiao

Department of Medicine, Division of Endocrinology and Metabolism; Institute for Human Genetics; and Program in Craniofacial Biology (C.J.C., S.H., K.J., A.M., B.M.M., and E.C.H.); and the Biomedical Sciences Graduate Program (J.T.V. and E.C.H.); University of California, San Francisco, San Francisco, California 94143-0794

Bone is increasingly recognized as an endocrine organ that can regulate systemic hormones and metabolism through secreted factors. Although bone loss and increased adiposity appear to be linked clinically, whether conditions of increased bone formation can also change systemic metabolism remains unclear. In this study, we examined how increased osteogenesis affects metabolism by using an engineered G protein-coupled receptor, Rs1, to activate G_s signaling in osteoblastic cells in Coll(2.3)+/Rs1+ transgenic mice. We previously showed that these mice have dramatically increased bone formation resembling fibrous dysplasia of the bone. We found that total body fat was significantly reduced starting at 3 weeks of age. Furthermore, Coll(2.3)+/Rs1+ mice showed reduced O₂ consumption and respiratory quotient measures without effects on food intake and energy expenditure. The mice had significantly decreased serum triacylglycerides, leptin, and adiponectin. Resting glucose and insulin levels were unchanged; however, glucose and insulin tolerance tests revealed increased sensitivity to insulin. The mice showed resistance to fat accumulation from a high-fat diet. Furthermore, Coll(2.3)⁺/Rs1⁺ mouse bones had dramatically reduced mature adipocyte differentiation, increased Wingless/Int-1 (Wnt) signaling, and higher osteoblastic glucose utilization than controls. These findings suggest that osteoblasts can influence both local and peripheral adiposity in conditions of increased bone formation and suggest a role for osteoblasts in the regulation of whole-body adiposity and metabolic homeostasis. (Endocrinology 157: 1481-1494, 2016)

ncreased bone marrow adiposity and bone fragility are 2 characteristics shared by aging, obesity, and diabetes (1, 2). This correlation suggests a role for adipocytes in osteoblast regulation and diseases of bone loss such as osteoporosis (3). Several previous studies focused on the link between increased adiposity and bone loss (2, 4, 5). However, our understanding of how the converse scenario of increased osteogenesis on adiposity and systemic energy consumption remains limited.

Glucose is thought to be the main source of energy for osteoblasts during mineralization and development (6, 7). Furthermore, osteoblasts are the primary source of osteocalcin (8–10), an important bone molecule that

can exist in 2 forms: a carboxylated form that is a bone matrix protein produced by osteoblasts and a decarboxylated form that acts as a systemic hormone to regulate metabolic homeostasis by regulating insulin sensitivity (11, 12). Although murine studies clearly demonstrate a role of decarboxylated osteocalcin in glucose regulation, clinical research studies in humans have only identified a correlative link between elevated serum osteocalcin levels and increased insulin sensitivity (12–16).

G protein-coupled receptor (GPCR) signaling is important for glucose homeostasis and vital for the development of both osteoblasts and adipocytes (17–19).

ISSN Print 0013-7227 ISSN Online 1945-7170
Printed in USA
Copyright © 2016 by the Endocrine Society
Received October 13, 2015. Accepted February 16, 2016.
First Published Online February 22, 2016

Abbreviations: BMC, bone mineral content; BMD, bone mineral density; CLAMS, Comprehensive Lab Animal Monitoring System; GAPDH, glyceraldehyde-3-phosphate dehydrogenase; GPCR, G protein-coupled receptor; H&E, hematoxylin and eosin; HFD, high-fat diet; PAI-1, plasminogen activator inhibitor-1; qPCR, quantitative polymerase chain reaction; RQ, respiratory quotient; TAG, triacylglyceride; Wnt, Wingless/Int-1 family.

GPCRs recognize extracellular signals and activate trimeric G proteins. Parathyroid hormone and Frizzled receptors, as well as the tyrosine kinase receptor for insulin, are important anabolic signals for bone and can increase glucose utilization (20-22). β-Adrenergic or adenosine receptors can increase or decrease adipogenesis, respectively (17). Studying the function of individual GPCRs can be challenging because many GPCRs can activate different $G\alpha$ subunits such as G_s and G_i , which increase or decrease cAMP production, respectively (20). Additionally, individual GPCRs can have both activating and inhibitory effects depending on cell type, and there may be potential redundancy between different GPCRs expressed in the same cell (20). Furthermore, loss of G_s-GPCR signaling in osteoblastic cells can cause increased adipogenesis in the bone, indicating an important role for osteoblastic G_s-GPCR signaling in regulating cell fate decisions (23).

Previously, we developed an engineered $G_s\alpha$ -coupled serotonin receptor, Rs1, based on a mutation that causes loss of reactivity to the endogenous ligand (serotonin) but retains constitutive basal activity and response to synthetic agonists (24). Mice expressing Rs1 under the control of the osteoblastic cell-specific Collagen 1a1 2.3-kb promoter fragment in a double-transgenic expression system (ColI(2.3)⁺/Rs1⁺ mice) had massive increases in overall bone mass (24–26). Here, we use these ColI(2.3)⁺/Rs1⁺ mice to examine how osteoblastic G_s -GPCR-coupled signaling affects glucose metabolism, peripheral adiposity, and bone marrow adiposity.

Materials and Methods

Animal studies

All mouse studies were approved by the Institutional Animal Care and Use Committee and the Laboratory Animal Research Center at the University of California, San Francisco. The ColI(2.3)-tTA/TetO-Rs1 double transgenic mice (abbreviated ColI2.3+/Rs1+ mice, and maintained on the FVB/N background) were generated as before by crossing ColI(2.3)-tTA mice (MMRRC 029992) with TetO-Rs1 mice (MMRRC 030758) and maintained on regular chow to allow continuous expression of the Rs1 transgene (24). Only male mice were used in this study to minimize sex-dependent differences in metabolism.

Bone densitometry and imaging

Dual energy x-ray absorptiometry on a GE Lunar Piximus2 was used to measure mouse whole-body areal bone mineral density (BMD) and bone mineral content (BMC). Mice were anesthetized with inhaled isofluorane (1.5%–2% in oxygen) and scanned at the times indicated.

Analysis of whole-body fat

Whole-body fat and lean mass were measured using an EchoMRI-100 (Echo Medical Systems) on live mice or on individual tissues freshly dissected from euthanized mice. Whole-body fat and lean mass were normalized to body weight to calculate the percent body fat and lean mass.

Metabolism assessments

An Oxymax/Comprehensive Lab Animal Monitoring System (CLAMS) (Columbus Instruments) was used to measure O_2 consumption, CO₂ production, respiratory quotient (RQ), energy expenditure, ambulatory activity, water, and food consumption. O2 consumption, CO2 production, RQ, and energy expenditure were all normalized to lean mass. Mice were individually housed and provided with regular food and water for 5 days. For high-fat diet (HFD) analysis, we used the energy balance equation: total energy expenditure = average food intake + change in somatic energy (27, 28). Change in somatic energy was determined between 3 and 8 weeks of age by the following formula: change in somatic energy storage = (pF)(F) + (pFFM)(FFM), where pF =9.4 kcal/g is the energy density for fat mass, pFFM = 1.8 kcal/gis the energy density for fat-free mass, F = the change in fat mass from 3 to 8 weeks, and FFM = the change in fat-free mass between 3 and 8 weeks of age (28).

Paired feeding

After weaning, control and ColI2.3⁺/Rs1⁺ mice were subjected to paired feeding for 7 weeks, in which mice received measured amounts of food with free access to water and enrichment (29). Diets of control mice and ColI2.3⁺/Rs1⁺ mice were measured daily. Control mice were then fed the same amount of food as ColI2.3⁺/Rs1⁺ mice consumed on the previous day until the end of the study.

High-fat diet

Control and ColI2.3⁺/Rs1⁺ mice were given either a 22% fat diet (regular chow; PicoLab 5058M) or a 60% fat diet (high-fat chow; Research Diets D12492) starting at 3 weeks of age and maintained until 8.5 weeks of age. Food consumption was measured twice each week.

Histology

Inguinal and gonadal adipose tissues

Adipose tissues from 8-week-old control and ColI2.3⁺/Rs1⁺ mice were placed in neutral buffered formalin for at least 24 hours and then replaced with 70% ethanol for at least 24 hours before paraffin embedding, sectioning, and staining with hematoxylin and eosin (H&E), using standard protocols (Gladstone Institutes Histology Core). For adipocyte and lipid storage quantification, 6 photos per mouse from each tissue were counted. Lipid area was quantified using ImageJ (30) to calculate the white area per slide, then expressed as a percent of white area per slide divided by the number of adipocytes.

Femur and tibia bones

Femur and tibia bones were collected in neutral buffered formalin before decalcification using 10% EDTA. Bones were par-

affin embedded and sectioned at the midline, then stained with H&E.

Bone triacylglyceride (TAG) analysis

Serum, femurs, and tibias were collected and incubated in a 2:1 chloroform (Sigma): methanol (Sigma) solution overnight. After incubation, the organic layer was separated from the aqueous layer and air dried with nitrogen gas. The remaining dried samples were resuspended in Triton X-100 and aliquots were run in triplicate with Infinity Triglycerides Reagent (Thermo). Samples were incubated for 30 minutes and then measured with a microplate reader (BioTek Instruments) at 500 nm and calibrated according to a TAG standard (Pointe Scientific, Inc). Samples were normalized to protein levels in the aqueous layer using a Peirce BCA Protein Assay kit (Thermo).

Blood and serum analysis

Blood glucose measurements were taken immediately after whole blood isolation from overnight-fasted mice using a One Touch glucose meter. Blood was collected from euthanized mice by cardiac puncture. Samples were allowed to clot for 30 minutes and centrifuged for 10 minutes at 2000 revolutions per minute before storage at -80° C. Serum was analyzed by ELISA for insulin (Millipore) or for carboxylated and decarboxylated osteocalcin (Takara/Clonetech Biosciences) according to the manufacturer's instructions and detected on a luminescent plate reader (Biotek Synergy 2) to measure absorbance at 560 nm. Serum analysis of ghrelin, PAI-1 (plasminogen activator inhibitor-1), resistin, leptin, and adiponectin were performed by Eve Technologies.

Glucose and insulin tolerance tests

Eight- and 10-week control and ColI(2.3)⁺/Rs1⁺ mice were fasted overnight or for 4–5 hours for glucose and insulin tolerance tests, respectively (31). Mice were then weighed and an initial glucose measurement was taken. Mice were then given an ip injection of either 2-g/kg body weight of glucose or 0.75-U/kg body weight of insulin (HumulinR U-100; Lilly). Blood glucose measurements from the tail vein were then taken at 15, 30, 45, 60, 90, and 120 minutes.

RNA isolation, cDNA synthesis, and quantitative PCR

Whole femur, tibia, inguinal, and gonadal tissues were cleaned of excess tissue, placed in TRIzol (Invitrogen), and homogenized using a Powergen 125 homogenizer (Fisher). Whole femur and tibia were used for quantitative polymerase chain reaction (qPCR) analysis because the ColI2.3⁺/Rs1⁺ mouse

bone marrow cavity is severely disrupted, making it difficult to consistently separate osteoblasts adherent to a bone surface from hematopoietic bone marrow components from ColI2.3⁺/Rs1⁺ bones. RNA was isolated using chloroform extraction for all tissues. cDNA was synthesized with oligo dT primers with the Superscript III (Invitrogen) kit as described (32). qPCR expression analysis was performed using TaqMan primers for qPCRs (Supplemental Table 1) on a Viia7 real-time thermocycler (Applied Biosystems) run in 5- μ L sample volumes in triplicate. All expression values were normalized to *Gapdh* (glyceraldehyde-3-phosphate dehydrogenase) expression.

Western blotting

Antibodies against total β -catenin (D10A8; Cell Signaling) and nonphospho-(active) β -catenin (D13A1; Cell Signaling) were used to probe Western blottings of total protein isolated from frozen femurs in Pierce radioimmunoprecipitation assay lysis and extraction buffer (Thermo). Antibodies against GAPDH (GA1R; Thermo Fisher) were used as a loading control. Antibodies bound to β -catenin and GAPDH were detected with horseradish peroxidase-conjugated secondary antibodies (Rockland and Jackson ImmunoResearch). Images were taken on an ImageQuant 4000 (GE Healthcare). All antibodies used in this study are listed in Table 1.

Seahorse metabolic assessment

Bone chips from crushed femurs, tibias, and hip bones were washed twice to remove hematopoietic cells and digested in collagenase as described (33). Released bone cells were seeded directly into an XFe24 well plate and grown for 7 days in culture. Cells were then subjected to a mitochondrial stress test using oligomycin, trifluorocarbonylcyanide phenylhydrazone, rotenone, and antimycin A (Seahorse Biosciences). Glycolysis stress tests were also conducted using oligomycin and 2-deoxy-D-glucose (Seahorse Biosciences). After each analysis, total protein content was quantified (Peirce BCA kit), and normalized to $\rm O_2$ consumption rate or extracellular acidification rate, respectively.

Statistical analysis

All data are represented as mean \pm 1 SD. Data were assumed to adhere to a normal distribution as this was evident in our BMD and BMC data sets using the Kolmogorov-Smirnov test. Differences between the means of biological replicates for all samples were calculated using an unpaired 2-tailed t test (GraphPad Prism and Microsoft Excel). Analyses were considered statistically significant if $P \leq .05$.

Table 1. Antibody Table

Peptide/Protein Target	Antigen Sequence (if Known)	Name of Antibody	Manufacturer, Catalog Number, and/or Name of Individual Providing the Antibody	Species Raised in; Monoclonal or Polyclonal	Dilution Used
β-CATENIN	N/A	β-Catenin	Cell Signaling, D10A8 XP	Rabbit; monoclonal	1:1000
Active β -CATENIN	N/A	Nonphospho (active) β-Catenin (Ser33/37/Thr41)	Cell Signaling, D13A1	Rabbit; monoclonal	1:1000
GAPDH	N/A	GAPDH loading control antibody	Thermo, GA1R	Mouse; monoclonal	1:5000
Antirabbit IgG	N/A	Donkey antirabbit IgG-HRP conjugated	Rockland, NA9340V	Donkey; polyclonal	1:5000
Antimouse IgG	N/A	Peroxidase AffiniPure donkey antimouse IgG (H + L)	Jackson ImmunoResearch 715-035-151	Donkey; polyclonal	1:5000

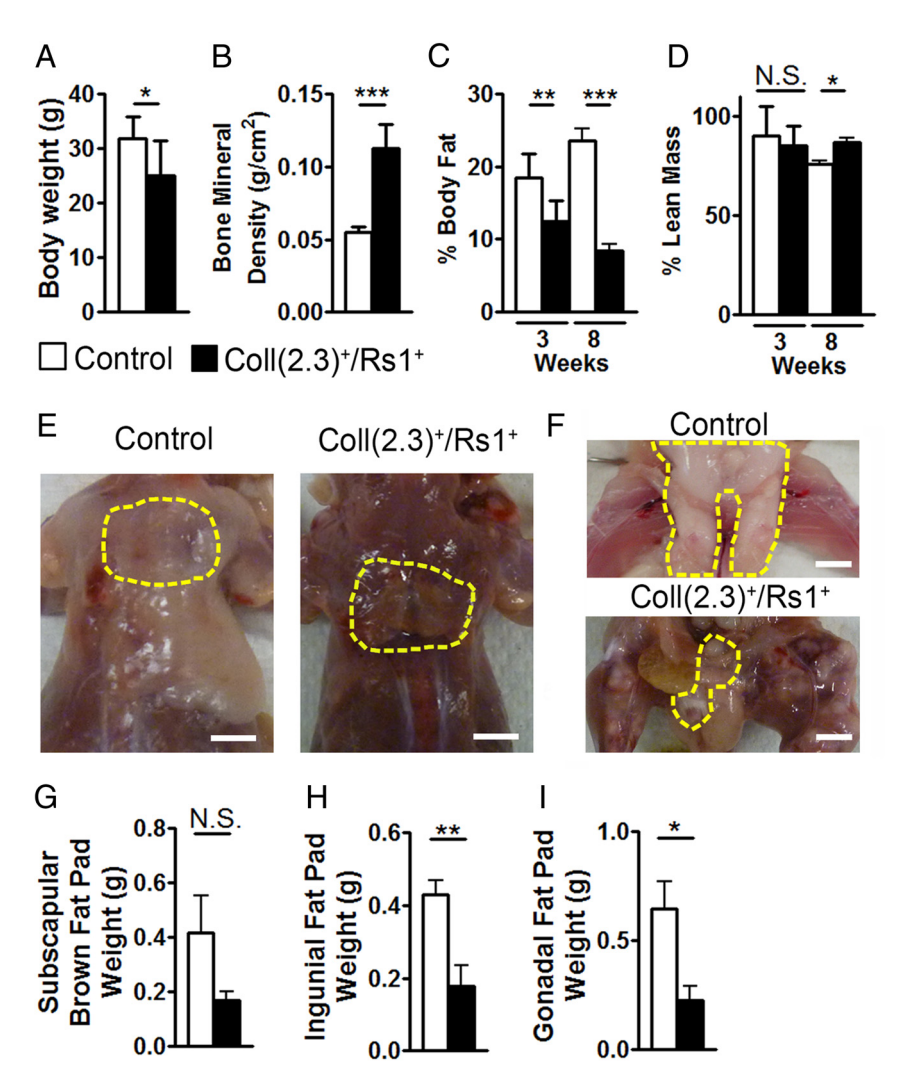


Figure 1. Osteoblastic G_s signaling reduces adipose tissue in Coll(2.3)⁺/Rs1⁺ mice. Body weight (A) and BMD (B) of 8- to 9-week-old control and Coll(2.3)+/Rs1+ male mice. Data are from n = 9 control and n = 6 (n = 5 for BMD) $Coll(2.3)^+/Rs1^+$ mice. Percent whole-body fat (C) and lean mass (D) of 3- and 8-week-old control and Coll(2.3)+/Rs1+ male mice. Data are from n = 7 control and $n = 4 \text{ Coll}(2.3)^+/\text{Rs1}^+$ male mice at 3 weeks of age, and n = 9control and $n = 6 \text{ Coll}(2.3)^+/\text{Rs1}^+$ male mice at 8 weeks of age. Representative dorsal (E) and ventral (F) photos of control and Coll(2.3)+/Rs1+ male mice showing reductions of visceral adipose tissues with no significant effect on subscapular brown adipose tissue. Yellow outlines denote brown and gonadal adipose tissues. Scale bar, 5 mm. Tissue weights of (G) subscapular brown, (H) inguinal, and (I) gonadal fat pads from 8- to 9-week-old male mice. Data are from n = 5 control and n = 6 Coll(2.3)⁺/Rs1⁺ male mice for brown and gonadal adipose tissue, and n = 4 control and n = 5 Coll(2.3)⁺/Rs1⁺ male mice for inguinal adipose tissue. Statistical differences were determined by Student's t test; *, P < .05; **, P < .01; ***, P < .001; N.S., not significant.

Results

Coll(2.3)+/Rs1+ mice have decreased total body fat

Osteoblast G_s-GPCR signaling in ColI(2.3)⁺/Rs1⁺ mice showed a significant reduction in total body weight but a 2-fold increase in BMD compared with control littermates, as previously reported (Figure 1, A and B) (24, 26). EchoMRI confirmed a significant decrease in wholebody fat starting at 3 weeks of age with a corresponding increase in lean mass by 8 weeks of age (Figure 1, C and D). Dissection of ColI(2.3)⁺/Rs1⁺ mice showed significant reductions in inguinal and gonadal white adipose tissues, but not subscapular brown adipose tissues (Figure 1, E-I). These findings indicated that $ColI(2.3)^+$ / Rs1⁺ mice showed changes in whole-body adiposity.

Coll(2.3)+/Rs1+ mice showed increased fat utilization by metabolic cage analysis

We next analyzed the whole-body metabolic requirements of these mice using CLAMS metabolic cages under thermoneutral conditions. Volume of oxygen (VO₂), volume of carbon dioxide (VCO₂), RQ, and energy consumption were normalized to lean mass to account for the slight decrease in body weight of ColI(2.3)⁺/Rs1⁺ mice compared with control mice. ColI(2.3)⁺/Rs1⁺ mice had marked reductions in O2 consumption with only small transient differences in CO₂ production (Figure 2, A and B). Interestingly, ColI(2.3)⁺/Rs1⁺ RQs were significantly lower (Figure 2C), suggesting increased fat utilization (34). Total energy expenditure was not significantly altered in ColI(2.3)⁺/ Rs1⁺ mice (Figure 2D). We found no significant differences in food and water intake, total ambulatory activity, or energy expenditure (Figure 2, E-H).

Coll(2.3)+/Rs1+ mice have increased insulin sensitivity

Osteoblastic cells can regulate insulin sensitivity through secretion of decarboxylated osteocalcin

(10-12, 35). Given the indications of increased fat utilization in ColI(2.3)⁺/Rs1⁺ mice during metabolic cage analysis, we examined glucose and insulin homeostasis in ColI(2.3)⁺/Rs1⁺ mice that were free fed a regular chow diet. Fasting blood glucose and insulin levels showed no major differences in the ColI(2.3)+/Rs1+ mice (Figure 3, A and B), despite known high expression of osteocalcin which has been reported to decrease fasting glucose levels in mice (35, 36). Insulin sensitivity

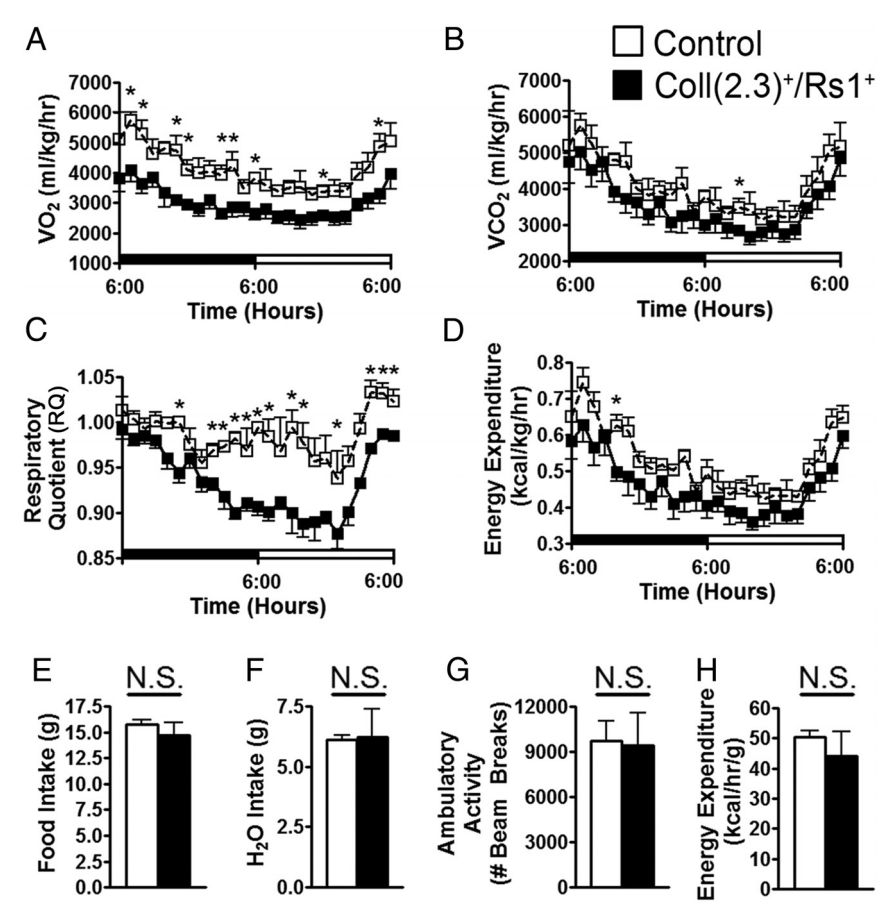


Figure 2. Coll(2.3)*/Rs1* mice have increased fat utilization. Volume of oxygen (VO₂) (A), volume of carbon dioxide (VCO₂) (B), respiratory quotient (RQ) (C), and energy expenditure (D) of 8-week-old male control and an Coll(2.3)*/Rs1* mice mouse subjected to a CLAMS on day 3, after 2 days of acclimation to the chamber. Total food intake (E), total water consumption (F), total ambulatory activity (G), and total energy expenditure (H) of 8-week-old control and Coll(2.3)*/Rs1* mice after 5 days in the CLAMS. Data are from n=3 control and n=5 Coll(2.3)*/Rs1* male mice. Statistical differences were determined by Student's t test; *, t < .05; N.S., not significant.

was not affected using the homeostatic model assessment of insulin resistance calculation (Figure 3C). However, serum TAG levels were significantly reduced in ColI(2.3)⁺/Rs1⁺ mice, which is in line with the reduction in white adipose tissues and increased fat utilization by metabolic cage analysis seen previously (Figures 1, 2, and 3D).

We next tested for alterations to glucose homeostasis using dynamic glucose and insulin tolerance tests. Glucose levels in $ColI(2.3)^+/Rs1^+$ mice peaked similarly to control littermates but returned to normal levels more quickly than control littermates (Figure 3E). Insulin tolerance tests revealed higher insulin sensitivity in $ColI(2.3)^+/Rs1^+$ mice than control littermates (Figure 3F).

Although our metabolic cage analysis suggested no significant differences in food intake, we pair fed ColI(2.3)⁺/Rs1⁺ and control mice for 7 weeks starting at 3 weeks of age. We confirmed that the reductions in

inguinal and gonadal adipose tissues were still present and independent of food intake (Figure 3, G-K). Furthermore, $ColI(2.3)^+/$ Rs1⁺ mice that were pair fed a regular chow diet showed an increase in insulin sensitivity similar to that seen in ColI(2.3)⁺/Rs1⁺ mice free fed a regular chow diet (Figure 3, L and M). These results indicated that fasting glucose and insulin levels are unaffected in $ColI(2.3)^+$ / Rs1⁺ mice. Furthermore, dynamic testing revealed increased insulin sensitivity in ColI(2.3)⁺/Rs1⁺ mice and that the metabolic changes do not arise from alteration to food intake.

Coll(2.3)⁺/Rs1⁺ mice are resistant to fat accumulation and bone density loss when fed a HFD

We next tested whether ColI(2.3)⁺/Rs1⁺ mice might be resistant to the fat accumulation caused by a HFD. We fed ColI(2.3)⁺/Rs1⁺ mice a HFD starting at 3 weeks of age (Figure 4, A and B). The ColI(2.3)⁺/Rs1⁺ mice showed slight reductions in food intake over the 5 weeks, but when normalized to body size, food intake showed no significant differ-

ences (Figure 4C). ColI(2.3)⁺/Rs1⁺ mice on a HFD showed no alterations in body weight as compared with controls; however, whole-body fat was significantly reduced with corresponding increases in lean mass, BMD, and BMC (Figure 4, D and E). Interestingly, control mice fed a HFD had significant reductions in BMD and BMC that were not seen in ColI(2.3)⁺/Rs1⁺ mice, suggesting that the ColI(2.3)⁺/Rs1⁺ bone growth was not affected by higher caloric intake (Figure 4E). Although ColI(2.3)⁺/Rs1⁺ mice free fed a regular diet showed no differences in body composition, control mice on a HFD showed increased whole-body fat with decreased lean mass. Fasting serum glucose was higher in ColI(2.3)⁺/Rs1⁺ mice on a HFD but not in control mice on a HFD (Figure 4F).

Examination of ColI(2.3)⁺/Rs1⁺ inguinal, gonadal, and subscapular brown adipose tissue mass showed similar reductions in free-fed ColI(2.3)⁺/Rs1⁺ mice and HFD mice, without affecting brown adipose tissue (Fig-

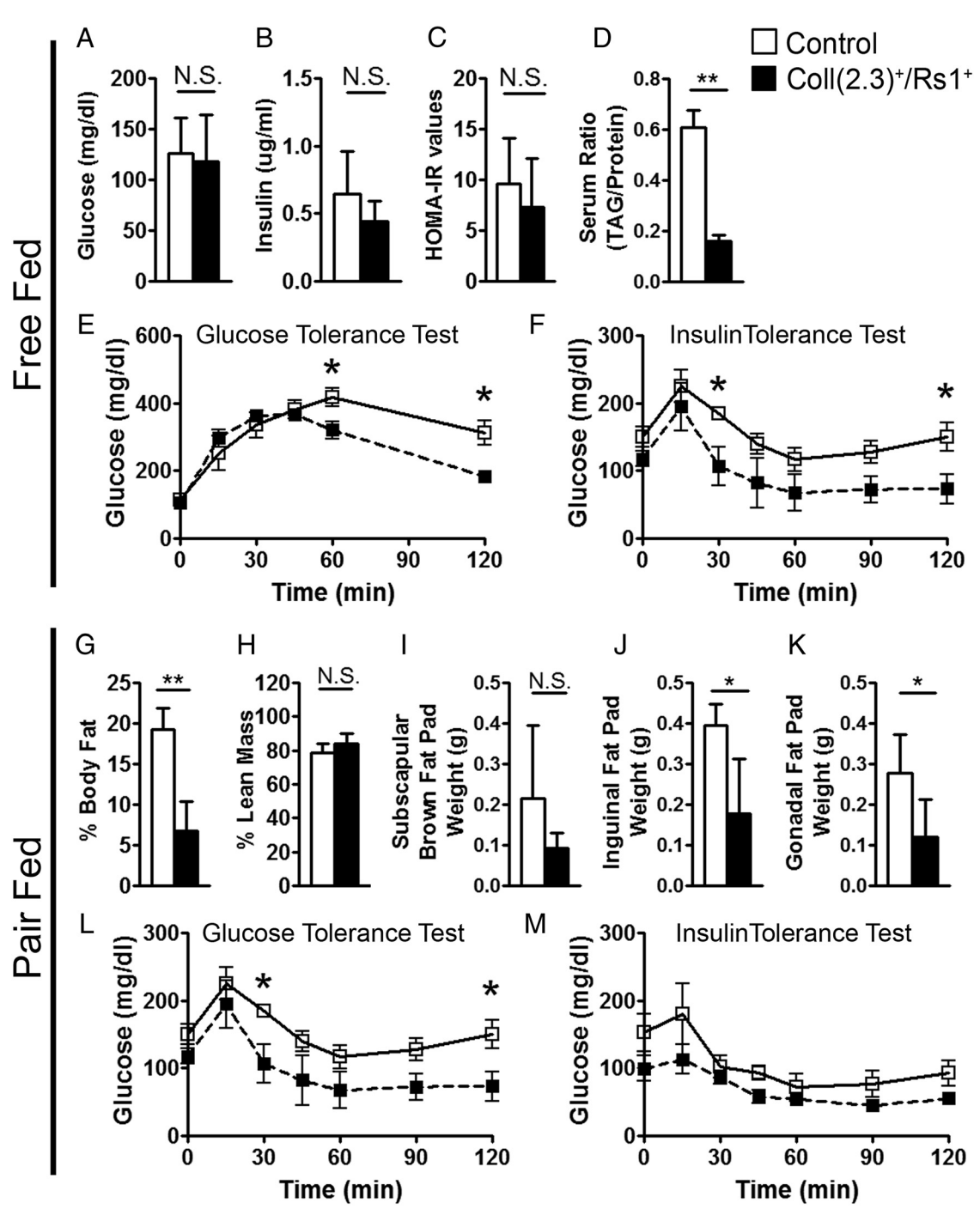


Figure 3. Coll(2.3)+/Rs1+ mice have increased insulin sensitivity. Fasting serum glucose (A) and insulin (B) of 8- to 9-week-old control and Coll(2.3)+/Rs1+ male mice. C, Homeostatic model assessment of insulin resistance (HOMA-IR) of 8- to 9-week-old male control and Coll(2.3)+/Rs1+ mice. Data are from n = 6-11 control and n = 4-8 Coll(2.3)+/Rs1+ mice. D, Ratio of serum TAGs to serum protein of 8- to 9-week-old control and Coll(2.3)+/Rs1+ male mice. Data are from n = 4 control and n = 3 Coll(2.3)+/Rs1+ mice. Glucose (E) and insulin (F) tolerance test of mice injected with 2 g/kg of glucose (at 8 wk of age) or 0.75-U/kg body weight of insulin (at 10 wk of age), respectively. Data are from n = 6 control and n = 4 Coll(2.3)+/Rs1+ male mice. Control and Coll(2.3)+/Rs1+ mice in A-F are all free fed with regular chow. Whole-body fat (G) and lean body mass (H) of male 8- to 10-week-old control and Coll(2.3)+/Rs1+ mice subjected to paired feeding with regular chow starting at 3 weeks of age. Tissue weights of (I) subscapular brown, (J) inguinal, and (K) gonadal fat pads from 8- to 10-week-old male mice subjected to paired feeding starting at 3 weeks of age. Glucose (L) and insulin (M) tolerance tests of pair fed male mice. Data are from n = 3-4 control and n = 4-6 Coll(2.3)+/Rs1+ mice. Statistical differences were determined by Student's t test; *, t < .05; ***, t < .01; ***, t < .001; N.S., not significant.

ure 4G). Whole-body metabolic energy balance measurements (energy balance equation: total energy expenditure = average food intake + change in somatic

energy) (27, 28) showed that ColI(2.3)⁺/Rs1⁺ mice had significantly reduced somatic energy storage between 3 and 8 weeks of age on a HFD (Figure 4H). We found no

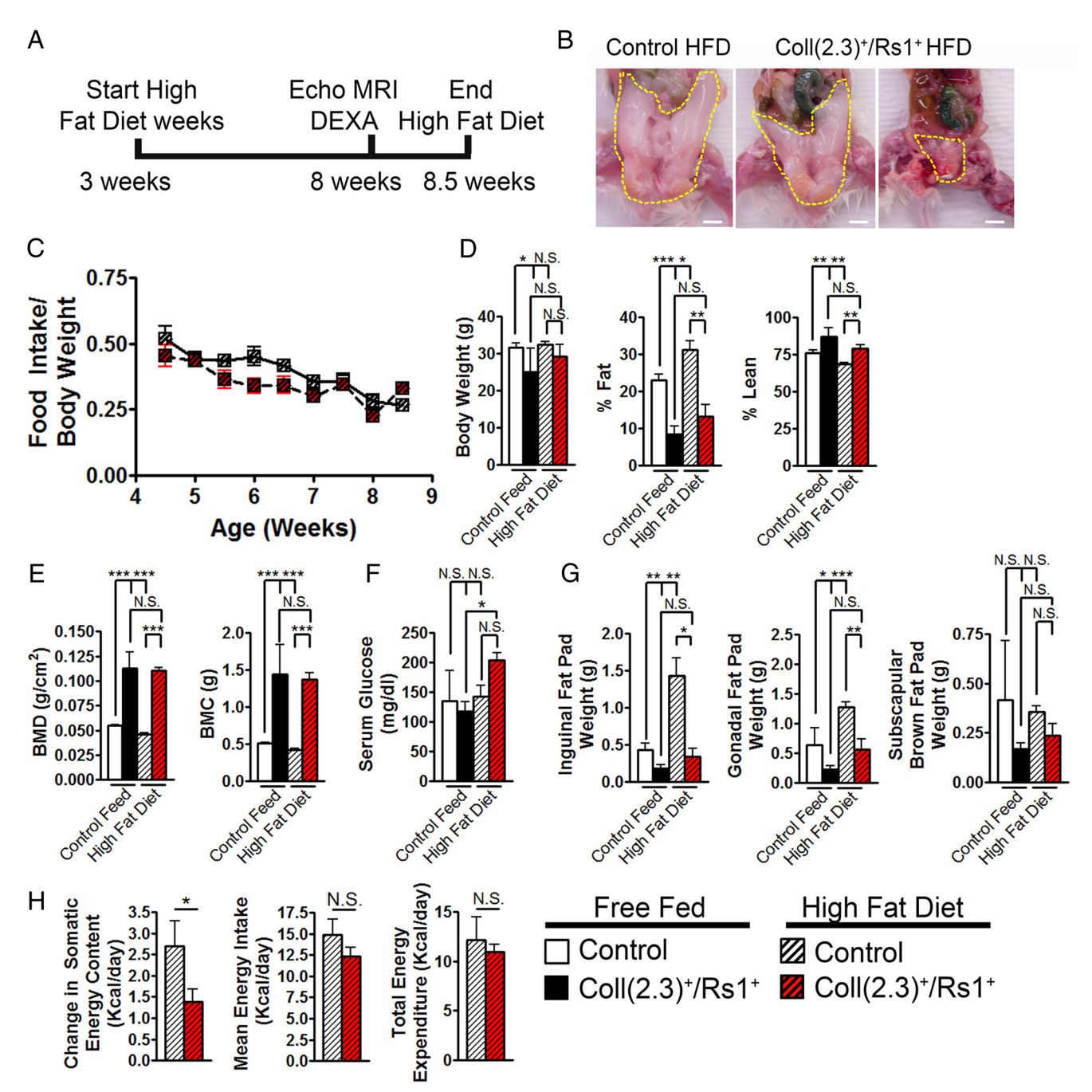


Figure 4. Coll(2.3)+/Rs1+ mice on a HFD are resistant to increases in adiposity. A, Male control and Coll(2.3)+/Rs1+ mice were fed a HFD starting at 3 weeks of age and followed for 5.5 weeks. B, Representative ventral photos of adipose tissues from 1 control and 2 Coll(2.3)+/Rs1+ mice fed a HFD for 5.5 weeks. C, Whole-body weight normalized to food intake. D, Whole-body weight, percent body fat, and percent lean body mass of 8-week-old control and Coll(2.3)+/Rs1+ mice free fed a regular chow diet or a HFD for 5 weeks. E, BMD and BMC male 8-week-old control and Coll(2.3)+/Rs1+ mice free fed a regular chow diet or a HFD for 5 weeks. Coll(2.3)+/Rs1+ mice. F, Serum glucose from 8- to 9-week-old male mice free fed a regular chow diet or a HFD. G, Tissue weights of inguinal, gonadal, and subscapular brown fat pads from 8- to 9-week-old mice free fed a regular chow diet or a HFD. Data are from n = 10-14 control and n = 5-8 Coll(2.3)+/Rs1+ male mice free fed a regular chow diet and n = 9 control and n = 4 Coll(2.3)+/Rs1+ male mice fed a HFD. H, Change in somatic energy content, mean energy intake, and energy expenditure of control and Coll(2.3)+/Rs1+ mice fed a HFD between 3 and 8 weeks of age. Data are from n = 4 control and n = 4 Coll(2.3)+/Rs1+ male mice fed a HFD. Statistical differences were determined by Student's t test; t, t, t cols; t cols; t cols, t col

significant differences in average energy intake or energy expenditure, consistent with our CLAMS studies (Figure 2). These results indicate that ColI(2.3)⁺/Rs1⁺ mice bone growth is unaffected by caloric intake and that ColI(2.3)⁺/Rs1⁺ mice are resistant to diet-induced obesity.

White adipose tissues are reduced in size, but differentiation is not altered in Coll(2.3)⁺/Rs1⁺ peripheral adipocytes

We next examined the inguinal and visceral gonadal adipose tissues in free-fed and HFD-fed mice. Both

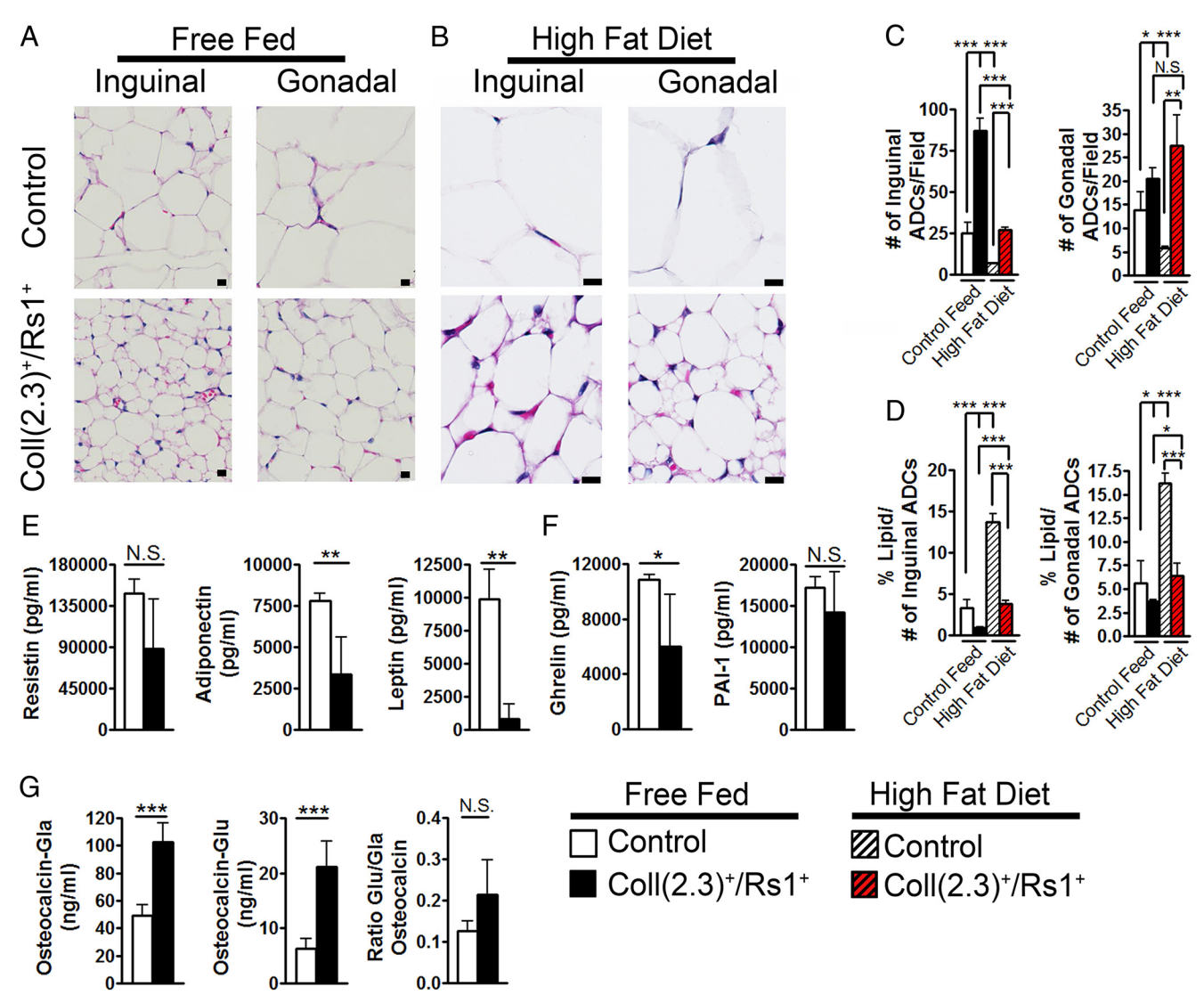


Figure 5. Coll(2.3)+/Rs1+ mice have smaller adipocytes, reduced levels of serum adipogenic factors, and increased levels of serum osteocalcin. H&E-stained histological sections of (A) free-fed and (B) HFD-fed inguinal and gonadal adipose tissue in male 8-week-old control and Coll(2.3)+/Rs1+ mice. Scale bar, 10 μ m. Histological counts of adipocytes from inguinal and gonadal adipose tissues (C) and histological counts normalized to % lipid content (D). Data in C and D are from 12 fields of 2 individual control and 2 individual Coll(2.3)+/Rs1+ male mice on a free fed or HFD. E, Serum resistin, adiponectin, and leptin. F, Serum ghrelin and PAI-1 from male 8- to 9-week-old control and Coll(2.3)+/Rs1+ mice. Data are from male n = 6 control and n = 5 Coll(2.3)+/Rs1+ male mice. G, Serum carboxylated osteocalcin, decarboxylated osteocalcin, and the ratio of decarboxylated to carboxylated osteocalcin from male 8- to 9-week-old control and Coll(2.3)+/Rs1+ mice. Data are from n = 5 control and n = 6 Coll(2.3)+/Rs1+ male mice. Statistical differences were determined by Student's t test; *, P < .05; ***, P < .01; ****, P < .001; N.S., not significant.

ColI(2.3)⁺/Rs1⁺ inguinal and gonadal adipocytes were reduced in size with increased numbers of adipocytes per field and decreased lipid content (Figure 5, A–D). Histological analysis of inguinal and gonadal tissues of ColI(2.3)⁺/Rs1⁺ mice on a HFD revealed an increase in adipocytes compared with control and ColI(2.3)⁺/Rs1⁺ mice that were free fed a regular chow diet; however, adipocytes in the inguinal and gonadal tissues of ColI(2.3)⁺/Rs1⁺ mice were still reduced in size (Figure 5, C and D).

Gene expression analysis of gonadal fat pads showed no significant differences in $Ppar\gamma$, $Cebp\alpha$, $Cebp\beta$, and $Cebp\delta$ expression (Supplemental Figure 1A and Ref. 37).

Expression of secreted adipogenic factors Adipoq, Pref1, and Lep were also not significantly altered in $ColI(2.3)^+/Rs1^+$ mice (Supplemental Figure 1B). Mesenchymal stem cell and adipocyte cell surface receptor RNA expression (Lepr and $Pdgfr\beta$), as well as TAG synthesis genes Dgat1 and Dgat2, lipolysis genes Atgl and Lipe (38, 39), and the fatty acid transporter Fabp4, also were not expressed differently in $ColI(2.3)^+/Rs1^+$ mice (Supplemental Figure 1, C-E). These results suggest that osteoblast G_s -GPCR signaling in $ColI(2.3)^+/Rs1^+$ mice can alter white adipose tissue size and lipid utilization, but does not alter the expression of genes associated with adipogenesis, lipolysis, or lipid synthesis.

Coll(2.3)⁺/Rs1⁺ mice have reduced serum adipokines with increased carboxylated and decarboxylated osteocalcin

We next determined whether serum metabolic factors and adipokines were altered in ColI(2.3)⁺/Rs1⁺ mice. Serum levels of resistin were not significantly altered, but both adiponectin and leptin were dramatically reduced (Figure 5E). We also found that ghrelin was significantly reduced in ColI(2.3)⁺/Rs1⁺ mice despite the absence of an effect on food consumption (Figure 5F). PAI-1, a marker of metabolic syndrome, was not significantly altered in ColI(2.3)⁺/Rs1⁺ mice (Figure 5F). Because decarboxylated osteocalcin can regulate both insulin sensitivity and adipose tissues (10, 35, 37), we measured serum carboxylated and decarboxylated osteocalcin and found that both were significantly increased in ColI(2.3)⁺/Rs1⁺ mice (Figure 5G). The ratio of decarboxylated to carboxylated osteocalcin was not significantly altered when compared with control mice (Figure 5G). These results suggest that the increased osteocalcin in ColI(2.3)⁺/Rs1⁺ mice may contribute to altered lipid and energy utilization in $ColI(2.3)^+/Rs1^+$ mice.

Reduced mature adipocytes in Coll(2.3)⁺/Rs1⁺ bones

Bone marrow adipocytes and osteoblasts are both thought to be derived from mesenchymal stem cells (40). Osteoblasts can secrete a variety of factors such as Wingless/Int-1 (Wnt) and osteocalcin proteins that can block adipogenesis (10, 41). We performed H&E staining on tibia and femur bones of 8-week-old ColI(2.3)⁺/Rs1⁺ mice along with TAG quantification to determine whether marrow adiposity was reduced in ColI(2.3)⁺/Rs1⁺ bones (Figure 6, A–D). Measurement of tibia and femur TAG to protein ratios confirmed a reduction in ColI(2.3)⁺/Rs1⁺ bone adiposity (Figure 6, B and D). Three-week-old ColI(2.3)⁺/Rs1⁺ mice showed no differences in adipocytes in the tibia (Supplemental Figure 2A). Markers of early adipogenesis (*Ppary* and *Cebp* α) were significantly increased in whole femurs, whereas $Cebp\beta$ and $Cebp\delta$ where not significantly altered (Figure 6E). We observed similar trends in ColI(2.3)⁺/Rs1⁺ tibias, but with a pronounced reduction in Cebpδ (Supplemental Figure 2, B-G). We observed no differences in Adipoq or Fabp4 message levels, but Pref1 was significantly increased, whereas *Lep* was not significantly decreased (Figure 6F). Furthermore, we saw increased expression of Lepr and Pdgfrβ (Figure 6G). Because bone marrow cells can also adopt properties of brown adipocytes (2, 42), we measured Ucp1 and Prdm16 expression. Ucp1 was not significantly altered, but Prdm16 expression was significantly increased, indicating that bone marrow adipocytes in $ColI(2.3)^+/Rs1^+$ bones may contain more brown adipose tissue differentiation as compared with control bones (Figure 6H). We also observed an increase in *Bglap* and *Col1a1* mRNA levels, and increased serum osteocalcin levels (Figure 6I and Supplemental Figure 3A), consistent with our previously reported findings. These data demonstrate that $ColI(2.3)^+/Rs1$ bones also show decreased adiposity and that increased G_s signaling in osteoblasts can affect the cell fate of adipogenic progenitor cells.

Bone adipogenesis is suppressed from up-regulation of Wnt signaling in Coll(2.3)⁺/Rs1⁺ mice

Because bone marrow adipocyte formation can be suppressed by Wnt signaling (41, 43), we next examined whether abnormalities in expression of Wnt genes (Wnt6, Wnt10a, and Wnt10b) may provide a potential mechanism for the decreased adipogenesis in ColI(2.3)+/Rs1+ mice. Wnt6, Wnt10a, and Wnt10b were all dramatically increased compared with control femurs (Figure 6I) and tibias (Supplemental Figure 3B). In addition to the upregulation of Wnt gene expression, we observed a significant up-regulation of Wnt downstream targets Ccnd1, Tcf7, and Axin2 in $ColI(2.3)^+/Rs1^+$ mice femur (Figure 6K) and tibia bones (Supplemental Figure 3C). The Wnt pathway inhibitors *Dkk1* and *Sost* were both increased in ColI(2.3)⁺/Rs1⁺ bones but only *Sost* was significantly increased in femurs, indicating that the bones may be attempting to compensate by decreasing Wnt expression (Figure 6L). Interestingly, the tibia showed a significant increase in Dkk1 but not Sost gene expression (Supplemental Figure 3D). This may reflect differences in the composition between the femur and tibia bones. We next looked to see whether activation of Wnt signaling was occurring through canonical β -catenin signaling (5). We found up-regulation of both total and active forms of β-CATENIN compared with control femurs (Figure 6M). These results indicate that ColI(2.3)⁺/Rs1⁺ bones have dysregulated Wnt signaling, which contributes to the reduction in adiposity in the bone.

Increased glycolytic demand by Coll(2.3)⁺/Rs1⁺ osteoblastic cells

Osteoblasts are thought to be highly dependent on glucose metabolism (7, 11, 12, 44), yet the metabolic analyses of the $ColI(2.3)^+/Rs1^+$ mice suggested effects on both peripheral and bone marrow fat utilization. To test whether G_s -GPCR signaling in osteoblasts activates increased fatty acid metabolism, we used the Seahorse mitochondrial and glycolytic stress tests to examine the oxidative respiration and glycolytic activity of isolated bone cells cultured for 7 days. We observed no significant differences in oxidative

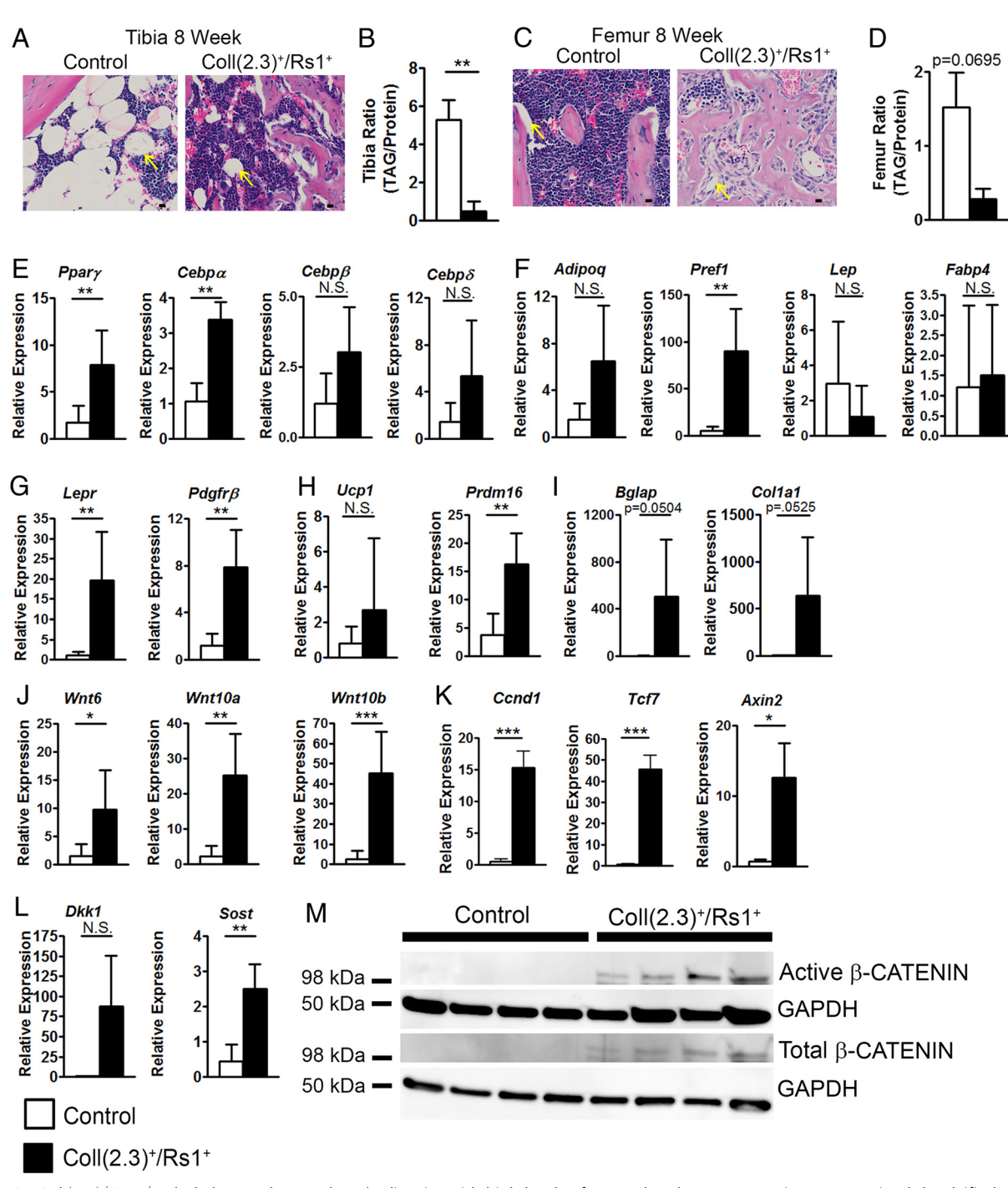


Figure 6. Coll(2.3)+/Rs1+ whole bones show reduced adiposity with high levels of Wnt related gene expression. H&E-stained decalcified 8-weekold tibia (A) and tibia TAG to protein ratio from control and Coll(2.3)+/Rs1+ male mice (B). H&E-stained decalcified 8-week-old femur (C) and femur TAG to protein ratio from control and Coll(2.3) $^+$ /Rs1 $^+$ male mice (D). Yellow arrows indicate adipocytes. Scale bar, 10 μ m. Serum TAGs are from n=6 control and n=4 Coll(2.3)⁺/Rs1⁺ male mice. E, qPCR of $Ppar\gamma$, $Cepb\alpha$, $Cepb\beta$, and $Cepb\delta$. Data are from n=3-5 control n=3-5and Coll(2.3)+/Rs1+ male mice. F, qPCR of adipogenic gene expression of Adipoq, Pref1, Lep, and Fabp4. Data are from n = 5-6 control and n = 5-6 cont 3–5 Coll(2.3)+/Rs1+ male mice. G, qPCR of mature adipogenic gene expression of Lepr and Pdqfr β . Data are from n = 5–6 control and n = 5 $Coll(2.3)^+/Rs1^+$ male mice. H, qPCR of brown adipose tissue genes Ucp1 and Prdm16. Data are from n=6 control and n=5 $Coll(2.3)^+/Rs1^+$ male mice. I, qPCR of Bglap and Col1a1. Data are from n = 5 control and n = 5 Coll(2.3)+/Rs1+ male mice. J, qPCR of Wnt6, Wnt10a, and Wnt10b. Data are from n = 6 control and n = 5 Coll(2.3) $^+$ /Rs1 $^+$ male mice. K, qPCR of Ccnd1, Tcf7, and Axin. Data are from n = 3-4 control and $n = 3 \text{ Coll}(2.3)^+/Rs1^+$ male mice. L, qPCR of Dkk1 and Sost. Data are from n = 3 control and $n = 5 \text{ Coll}(2.3)^+/Rs1^+$ male mice. M, Western blottings of active β -CATENIN and total β -CATENIN from crushed femurs with GAPDH as a loading control. Data are from n=4 control and n=64 Coll(2.3) $^+$ /Rs1 $^+$ male mice. Active β -CATENIN and GAPDH control images were taken at 45-second exposure. Total β -CATENIN and GAPDH control images were taken at 60- and 15-second exposures, respectively. All data are from crushed femurs of control and Coll(2.3)+/Rs1+ mice. Statistical differences were determined by Student's t test; *, P < .05; **, P < .01; ***, P < .001; N.S., not significant.

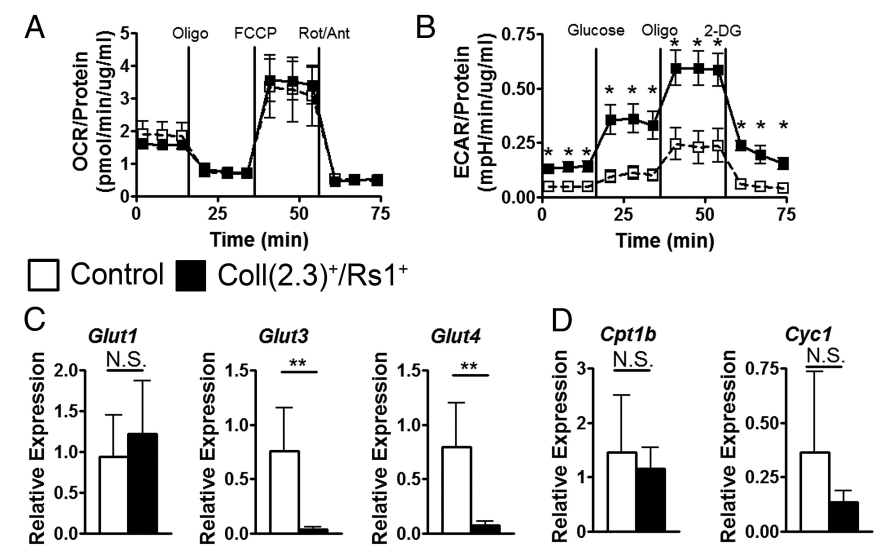


Figure 7. Coll(2.3)+/Rs1+ osteoblastic cells have increased glycolytic demand without alterations to oxidative metabolism. Seahorse (A) mitochondrial and (B) glycolytic stress tests of isolated bone cells cultured for 7 days. Data are from 5 wells from 2 separate male control mice and 6 wells from 3 separate male Coll(2.3)+/Rs1+ mice. C, *Glut1*, *Glut3*, and *Glut4* receptor expression from crushed tibias of control and Coll(2.3)+/Rs1+ mice. D, *Cpt1b* and *Cyc1* expression from crushed tibias of control and Coll(2.3)+/Rs1+ mice. Data are from n = 5 control and n = 5 Coll(2.3)+/Rs1+ male mice. Statistical differences were determined by Student's t = t test; t = t, t

respiration; however, we saw a pronounced increase in glycolytic activity in bone cells isolated from ColI(2.3)⁺/Rs1⁺ mice (Figure 7, A and B).

We next measured glucose and fatty acid transport receptors to see whether ColI(2.3)⁺/Rs1⁺ bones have differential expression of these genes. *Glut1* expression was not changed between control and ColI(2.3)⁺/Rs1⁺ bones, but *Glut3* and *Glut4* were dramatically reduced in ColI(2.3)⁺/Rs1⁺ bones (Figure 7C). *Ctn1b*, a fatty acid transporter, was not changed in ColI(2.3)⁺/Rs1⁺ bones (Figure 7D). Furthermore, a marker of oxidative respiration *Cyc1* showed no changes in expression in ColI(2.3)⁺/Rs1⁺ bone (Figure 7D). These results indicated that ColI(2.3)⁺/Rs1⁺ bone cells do not activate their oxidative phosphorylation pathway but have increased glycolytic demand, yet decreased expression of *Glut* transporters, specifically *Glut3* and *Glut4*.

Discussion

Our studies revealed that G_s -GPCR activity in osteoblastic cells can influence both bone and whole-body adiposity and metabolism. Within the bone, the increased total Wnt and osteocalcin expression in $ColI(2.3)^+/Rs1^+$ mice suggests that a noncell autonomous mechanism favors differentiation of mesenchymal progenitors to an osteogenic cell fate, but blocks maturation of mesenchymal progenitors into adipocytes. This latter block may result in increased

expression of early adipogenic genes (Figure 8). A similar model has been proposed in murine models with increased parathyroid hormone or parathyroid hormone related peptide acting on osteoblastic progenitor cells (45). In contrast, the mechanism for the reduction in systemic adiposity is less clear. However, our model with both activated G_s signaling in osteoblasts and high serum osteocalcin is consistent with the notion of bone as a regulator of peripheral glucose metabolism and fat utilization (44, 46).

Osteoblasts require a large amount of energy to produce mineralized bone (3, 7, 47). Furthermore, early osteogenic cells utilize oxidative phosphorylation, but at later stages of mineralization are more dependent on glycolytic metabolism (7). Although the ColI(2.3)⁺/Rs1⁺ mice

were previously shown to have large numbers of immature Osterix-positive cells (24) and produce large quantities of immature bone matrix (48), we found that the isolated bone cells had increased glucose metabolism but not fatty acid metabolism. Given the significantly increased number of osteoblastic-lineage cells in the CoII(2.3)⁺/Rs1⁺

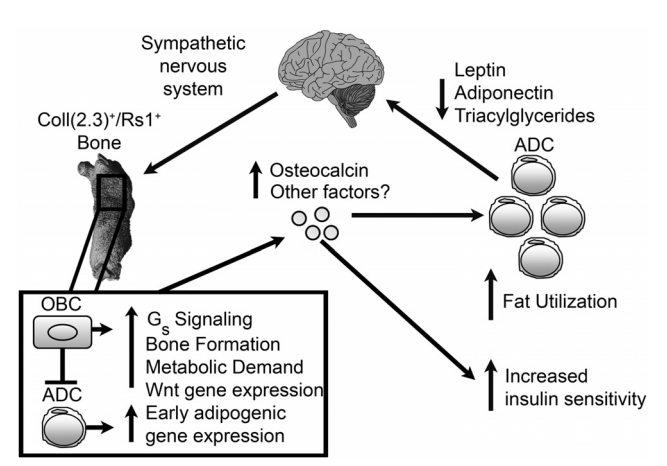


Figure 8. Model for the reduction of bone marrow and whole-body adiposity in $Coll(2.3)^+/Rs1^+$ mice. Osteoblastic (OBC) G_s -GPCR signaling in $Coll(2.3)^+/Rs1^+$ mice results in increased osteocalcin secretion that likely contributes to increased insulin sensitivity and influences fat utilization. This also reduces peripheral adiposity, serum TAGs, and secretion of adipokines by peripheral adipose tissues, which in turn affects sympathetic nervous system signaling to the bone and other tissues. In the $Coll(2.3)^+/Rs1^+$ mice bones, OBC G_s signaling results in reduced adipocytes development (ADCs) and increased OBC energy consumption, possibly from Wnt-mediated bone formation at the expense of adipogenesis.

Cain et al

mice, we speculate that this large mass increase reduces systemic adiposity by increasing total energy utilization. In addition, recent studies indicate that mature osteoblast glucose uptake via Glut1 may interact with Runx2 to regulate osteoblast differentiation (44). Our seemingly paradoxical finding of increased glucose utilization but decreased Glut3 and Glut4 expression may be a reflection of how the increased osteoblastic G_s-GPCR activity causes a shift of mesenchymal stem cells to the osteoblastic cell fate. We speculate that this change in cell fate also results in a reduction of the cells expressing Glut3 and Glut4 but leaves osteoblastic *Glut1* expression unchanged.

Although the increased osteocalcin levels we observed may have a modest effect on insulin sensitivity, it does not appear to be the primary mechanism for the reduction in adiposity in ColI(2.3)⁺/Rs1⁺ mice. In contrast to a previous report examining the effect of osteoclacin on fasting glucose (11), ColI(2.3)⁺/Rs1⁺ mice showed no differences in resting glucose, resting insulin levels, or total energy expenditure, but have reduced serum adipokines levels. Furthermore, ColI(2.3)⁺/Rs1⁺ mice are resistant to HFDinduced increases in fat, although we did find slightly increased fasting serum glucose levels on a HFD. Future work identifying which bone derived secreted factors in ColI(2.3) +/Rs1 + mice are capable of influencing adiposity will help us understand how osteoblastic G_c-GPCR ultimately affects adipose tissues, and also help in the development of novel treatments that then could potentially reduce systemic adiposity while having a favorable impact on bone health.

In previous studies, it has been shown that removing G_s or Wnt signaling in osteoblasts can increase bone marrow adipogenesis at the expense of osteogenesis (5, 23). Our studies suggest that the converse is also true: stimulating osteogenic metabolism through G_s-GPCR signaling in osteoblastic cells may be an approach for reducing adiposity. In addition, clinical studies with the GPCR-active drug teriparatide (recombinant parathyroid hormone) used to treat osteoporosis suggest that it can lower glycated hemoglobin (HbA1c) levels without affecting serum glucose (49, 50). Other studies also suggest that women treated with recombinant PTH for osteoporosis have increased levels of serum decarboxylated osteocalcin with a corresponding decrease in fat mass, which was also associated with improvements in BMI (46). Further delineation of this potential clinical correlation with GPCR signaling, and whether more specific GPCR pathway components might be targeted, is still needed.

ColI(2.3)⁺/Rs1⁺ mice display a more severe bone phenotype than that observed with other models of increased bone mass such as Col1-caPPR, Wnt10b, and FABP4-

Wnt10b transgenic mice (51-53). We have yet to identify the source of the elevated Wnt protein gene expression in ColI(2.3)⁺/Rs1⁺ bones. In addition, our findings are reminiscent of the phenotype observed in FABP4-Wnt10b transgenic mice, which also have reduced serum levels of leptin and resistin with increased insulin sensitivity (53). These mice also develop a significant bone phenotype, although levels of serum osteocalcin were not reported (54). Recently, Sinha et al demonstrated that loss of $G_s \alpha$ in osteoblastic cells results in increased adipogenesis at the expense of osteogenesis (23). These mice also had lower levels of Lef1 signaling, a measure of downstream Wnt signaling (32). Our results suggest that G_s signaling in osteoblastic cells may promote bone-mediated Wnt signaling activity, which may then play a role in the increased fat utilization seen in ColI(2.3)⁺/Rs1⁺ mice. However, the direct mechanistic link between peripheral fat mobilization and the increased glucose utilization of the ColI(2.3)⁺/Rs1⁺ osteoblasts remains to be elucidated.

In conclusion, we have identified that G_s-GPCR activity in osteoblastic cells can regulate systemic metabolic homeostasis in a model of significant increased bone growth, and lead to reduced bone marrow adiposity likely through increased Wnt signaling. Finally, we demonstrated that ColI(2.3)⁺/Rs1⁺ mice were resistant to increased adiposity when subjected to a HFD, which is most likely due to stimulated metabolic activity in osteoblastic cells. These studies have exciting implications for using engineered receptors to identify bone-derived factors that can regulate systemic energy utilization, which may help us develop new treatments for conditions of increased insulin resistance and bone fragility such as obesity and type 2 diabetes.

Acknowledgments

We thank Robert Nissenson, Mark Anderson, and Shingo Kajimura for valuable comments and discussion, Caroline Miller with the Gladstone Histology Core, and Christophe Paillart and the University of California, San Francisco (UCSF) Diabetes Research Center.

Address all correspondence and requests for reprints to: Edward C. Hsiao, MD, PhD, University of California, San Francisco, 513 Parnassus Avenue, HSE901G, San Francisco, CA 94143-0794. E-mail: edward.hsiao@ucsf.edu.

This work was supported in part by National Institutes of Health (NIH) Fellowship Training Grants 5T32GM007085-35, 5T32DK007418-34, and 5T32DK007161-41 (to C.J.C.), NIH Grant K08 AR056299 (to E.C.H.), NIH Grant R03 AR060986 (to E.C.H.), the UCSF Department of Medicine (to E.C.H.), and

a UCSF Diabetes and Endocrinology Research Center Pilot Grant (NIH P30 DK063720) (to E.C.H.).

Disclosure Summary: E.C.H. receives research funding from Clementia Pharmaceuticals for clinical trials unrelated to this work. The other authors have nothing to disclose.

References

- Rosen CJ, Ackert-Bicknell C, Rodriguez JP, Pino AM. Marrow fat and the bone microenvironment: developmental, functional, and pathological implications. Crit Rev Eukaryot Gene Expr. 2009;19: 109–124.
- 2. Krings A, Rahman S, Huang S, Lu Y, Czernik PJ, Lecka-Czernik B. Bone marrow fat has brown adipose tissue characteristics, which are attenuated with aging and diabetes. *Bone*. 2012;50:546–552.
- 3. Fazeli PK, Horowitz MC, MacDougald OA, et al. Marrow fat and bone–new perspectives. *J Clin Endocrinol Metab*. 2013;98:935–945.
- 4. Cao JJ. Effects of obesity on bone metabolism. *J Orthop Surg Res*. 2011;6:30.
- Song L, Liu M, Ono N, Bringhurst FR, Kronenberg HM, Guo J. Loss of wnt/β-catenin signaling causes cell fate shift of preosteoblasts from osteoblasts to adipocytes. J Bone Miner Res. 2012;27:2344– 2358.
- Yan W, Li X. Impact of diabetes and its treatments on skeletal diseases. Front Med. 2013;7:81–90.
- Guntur AR, Le PT, Farber CR, Rosen CJ. Bioenergetics during calvarial osteoblast differentiation reflect strain differences in bone mass. *Endocrinology*. 2014;155:1589–1595.
- 8. Kanazawa I, Yamaguchi T, Yamauchi M, et al. Serum undercarboxylated osteocalcin was inversely associated with plasma glucose level and fat mass in type 2 diabetes mellitus. *Osteoporosis Int.* 2011;22:187–194.
- Kanazawa I, Yamaguchi T, Tada Y, Yamauchi M, Yano S, Sugimoto T. Serum osteocalcin level is positively associated with insulin sensitivity and secretion in patients with type 2 diabetes. *Bone*. 2011; 48:720–725.
- Ferron M, McKee MD, Levine RL, Ducy P, Karsenty G. Intermittent injections of osteocalcin improve glucose metabolism and prevent type 2 diabetes in mice. *Bone*. 2012;50:568–575.
- Ferron M, Wei J, Yoshizawa T, et al. Insulin signaling in osteoblasts integrates bone remodeling and energy metabolism. *Cell*. 2010;142: 296–308.
- 12. Wei J, Karsenty G. An overview of the metabolic functions of osteocalcin. *Rev Endocr Metab Disord*. 2015;16:93–98.
- Booth SL, Centi A, Smith SR, Gundberg C. The role of osteocalcin in human glucose metabolism: marker or mediator? *Nat Rev Endocrinol*. 2013;9:43–55.
- Wang Q, Zhang B, Xu Y, Xu H, Zhang N. The relationship between serum osteocalcin concentration and glucose metabolism in patients with type 2 diabetes mellitus. *Int J Endocrinol*. 2013;2013:842598.
- 15. Ma XY, Chen FQ, Hong H, Lv XJ, Dong M, Wang QY. The relationship between serum osteocalcin concentration and glucose and lipid metabolism in patients with type 2 diabetes mellitus the role of osteocalcin in energy metabolism. *Ann Nutr Metab*. 2015;66: 110–116.
- 16. Gower BA, Pollock NK, Casazza K, Clemens TL, Goree LL, Granger WM. Associations of total and undercarboxylated osteocalcin with peripheral and hepatic insulin sensitivity and β-cell function in overweight adults. *J Clin Endocrinol Metab*. 2013;98: E1173–E1180.
- Eisenstein A, Ravid K. G protein-coupled receptors and adipogenesis: a focus on adenosine receptors. *J Cell Physiol*. 2014;229:414–421.

- 18. Blad CC, Tang C, Offermanns S. G protein-coupled receptors for energy metabolites as new therapeutic targets. *Nat Rev Drug Discov*. 2012;11:603–619.
- 19. Conklin BR, Hsiao EC, Claeysen S, et al. Engineering GPCR signaling pathways with RASSLs. *Nat Methods*. 2008;5:673–678.
- Wu M, Deng L, Zhu G, Li YP. G Protein and its signaling pathway in bone development and disease. Front Biosci (Landmark Ed). 2010;15:957–985.
- Esen E, Chen J, Karner CM, Okunade AL, Patterson BW, Long F. WNT-LRP5 signaling induces Warburg effect through mTORC2 activation during osteoblast differentiation. *Cell Metab*. 2013;17: 745–755
- 22. Zoidis E, Ghirlanda-Keller C, Schmid C. Stimulation of glucose transport in osteoblastic cells by parathyroid hormone and insulinlike growth factor I. *Mol Cell Biochem.* 2011;348:33–42.
- 23. Sinha P, Aarnisalo P, Chubb R, et al. Loss of Gsα early in the osteoblast lineage favors adipogenic differentiation of mesenchymal progenitors and committed osteoblast precursors. *J Bone Miner Res*. 2014;29:2414–2426.
- Hsiao EC, Boudignon BM, Chang WC, et al. Osteoblast expression of an engineered Gs-coupled receptor dramatically increases bone mass. *Proc Natl Acad Sci USA*. 2008;105:1209–1214.
- 25. Hsiao EC, Millard SM, Louie A, Huang Y, Conklin BR, Nissenson RA. Ligand-mediated activation of an engineered gs g protein-coupled receptor in osteoblasts increases trabecular bone formation. *Mol Endocrinol.* 2010;24:621–631.
- 26. Hsiao EC, Boudignon BM, Halloran BP, Nissenson RA, Conklin BR. Gs G protein-coupled receptor signaling in osteoblasts elicits age-dependent effects on bone formation. *J Bone Miner Res.* 2010; 25:584–593.
- 27. Ravussin Y, Gutman R, LeDuc CA, Leibel RL. Estimating energy expenditure in mice using an energy balance technique. *Int J Obes*. 2013;37:399–403.
- Guo J, Hall KD. Estimating the continuous-time dynamics of energy and fat metabolism in mice. PLoS Comput Biol. 2009;5:e1000511.
- Pan W, Ciociola E, Saraf M, et al. Metabolic consequences of ENPP1 overexpression in adipose tissue. *Am J Physiol Endocrinol Metab*. 2011;301:E901–E911.
- Parlee SD, Lentz SI, Mori H, MacDougald OA. Quantifying size and number of adipocytes in adipose tissue. *Methods Enzymol*. 2014; 537:93–122.
- 31. Ayala JE, Samuel VT, Morton GJ, et al. Standard operating procedures for describing and performing metabolic tests of glucose homeostasis in mice. *Dis Model Mech.* 2010;3:525–534.
- 32. Cain CJ, Manilay JO. Hematopoietic stem cell fate decisions are regulated by Wnt antagonists: comparisons and current controversies. *Exp Hematol.* 2013;41:3–16.
- 33. Schepers K, Hsiao EC, Garg T, Scott MJ, Passegué E. Activated Gs signaling in osteoblastic cells alters the hematopoietic stem cell niche in mice. *Blood*. 2012;120:3425–3435.
- Speakman JR. Measuring energy metabolism in the mouse theoretical, practical, and analytical considerations. Front Physiol. 2013;4:34.
- 35. Ferron M, Hinoi E, Karsenty G, Ducy P. Osteocalcin differentially regulates *β* cell and adipocyte gene expression and affects the development of metabolic diseases in wild-type mice. *Proc Natl Acad Sci USA*. 2008;105:5266–5270.
- Zhang Y, Zhou P, Kimondo JW. Adiponectin and osteocalcin: relation to insulin sensitivity. *Biochem Cell Biol*. 2012;90:613–620.
- 37. Kawai M, Devlin MJ, Rosen CJ. Fat targets for skeletal health. *Nat Rev Rheumatol*. 2009;5:365–372.
- 38. Ahmadian M, Wang Y, Sul HS. Lipolysis in adipocytes. *Int J Biochem Cell Biol*. 2010;42:555–559.
- Takeuchi K, Reue K. Biochemistry, physiology, and genetics of GPAT, AGPAT, and lipin enzymes in triglyceride synthesis. Am J Physiol Endocrinol Metab. 2009;296:E1195–E1209.

Cain et al

- 40. Kawai M, de Paula FJ, Rosen CJ. New insights into osteoporosis: the bone-fat connection. J Intern Med. 2012;272:317-329.
- 41. Cawthorn WP, Bree AJ, Yao Y, et al. Wnt6, Wnt10a and Wnt10b inhibit adipogenesis and stimulate osteoblastogenesis through a β-catenin-dependent mechanism. Bone. 2012;50:477-489.
- 42. Motyl KJ, Rosen CJ. Temperatures rising: brown fat and bone. Discov Med. 2011;11:179-185.
- 43. Tang QQ, Lane MD. Adipogenesis: from stem cell to adipocyte. Annu Rev Biochem. 2012;81:715-736.
- 44. Wei J, Shimazu J, Makinistoglu MP, et al. Glucose uptake and Runx2 synergize to orchestrate osteoblast differentiation and bone formation. Cell. 2015;161:1576-1591.
- 45. Datta NS, Abou-Samra AB. PTH and PTHrP signaling in osteoblasts. Cell Signal. 2009;21:1245-1254.
- 46. Schafer AL, Sellmeyer DE, Schwartz AV, et al. Change in undercarboxylated osteocalcin is associated with changes in body weight, fat mass, and adiponectin: parathyroid hormone (1-84) or alendronate therapy in postmenopausal women with osteoporosis (the PaTH study). J Clin Endocrinol Metab. 2011;96:E1982-E1989.
- 47. Lecka-Czernik B, Stechschulte LA. Bone and fat: a relationship of different shades. Arch Biochem Biophys. 2014;561:124-129.

- 48. Kazakia GJ, Speer D, Shanbhag S, et al. Mineral composition is altered by osteoblast expression of an engineered G(s)-coupled receptor. Calcif Tissue Int. 2011;89:10-20.
- 49. Niimi R, Kono T, Nishihara A, et al. Analysis of daily teriparatide treatment for osteoporosis in men. Osteoporos Int. 2015;26:2221.
- 50. Mazziotti G, Maffezzoni F, Doga M, Hofbauer LC, Adler RA, Giustina A. Outcome of glucose homeostasis in patients with glucocorticoid-induced osteoporosis undergoing treatment with bone active-drugs. Bone. 2014;67:175-180.
- 51. Calvi LM, Sims NA, Hunzelman JL, et al. Activated parathyroid hormone/parathyroid hormone-related protein receptor in osteoblastic cells differentially affects cortical and trabecular bone. J Clin Invest. 2001;107:277-286.
- 52. Wright WS, Longo KA, Dolinsky VW, et al. Wnt10b inhibits obesity in *ob/ob* and agouti mice. *Diabetes*. 2007;56:295–303.
- 53. Longo KA, Wright WS, Kang S, et al. Wnt10b inhibits development of white and brown adipose tissues. J Biol Chem. 2004;279:35503-
- 54. Bennett CN, Ouyang H, Ma YL, et al. Wnt10b increases postnatal bone formation by enhancing osteoblast differentiation. J Bone Miner Res. 2007;22:1924-1932.